

Value-Oriented Forecast Combinations for Unit Commitment

Mehrnoush Ghazanfariharandi, Robert Mieth

Industrial and Systems Engineering Department, Rutgers University, NJ, USA
{mehrnoush.ghazanfariharandi, robert.mieth}@rutgers.edu

Abstract—Value-oriented forecasts for two-stage power system operational problems have been demonstrated to reduce cost, but prove to be computationally challenging for large-scale systems because the underlying optimization problem must be internalized into the forecast model training. Therefore, existing approaches typically scale poorly in the usable training data or require relaxations of the underlying optimization. This paper presents a method for value-oriented forecast combinations using progressive hedging, which unlocks high-fidelity, at-scale models and large-scale datasets in training. We also derive a direct one-shot training model for reference and study how different modifications of the training model impact the solution quality. Our method reduces operation cost by 1.8% on average and trains forecast combinations for a 2736-bus test system with one year of data within 20 hours.

I. INTRODUCTION

Operational constraints of large-scale power plants require grid operators to decide on generator schedules ahead of time when load demand and weather-dependent generation are still uncertain. Hence, these scheduling decisions are made using forecasts of any uncertain quantities. Interestingly, “good” forecasts, measured by how well they match the true outcome, do not necessarily lead to better decisions [1], [2]. This aspect of forecasting is particularly acute in problems with asymmetric cost functions, as in critical infrastructure like power systems where the cost of resource shortage far exceed the cost of overage [3]. This observation has motivated research on *value-oriented* (or decision-focused) forecasting, where the quality of a forecast is measured by the value added to the decision [3]–[6].

Value-oriented forecasts offer a practical pathway to internalize more available information into the decision without modifying the decision-making process itself, e.g., through probabilistic forecasts and stochastic programming. (See also the discussion in [7].) Essentially, value-oriented forecasts are biased such that they improve the decision without altering the structure of the forecast and the decision-making problem itself. Value-oriented forecasting models can be trained by unifying the forecast model training problem and the decision-making problem as a bilevel program [3], [5], [6] or by integrating the decision-making problem into a gradient-descent training pipeline [4].

Existing approaches as in [3]–[6] suffer from poor scalability of the training problem and either remain small-scale or achieve practical scale through intricate heuristics or by

giving up modeling details. In this paper, we obtain value-oriented forecasts at scale even with high-fidelity models in the training phase using progressive hedging (PH). In particular, we take the perspective of a power system operator that has access to point forecasts of uncertain demand and renewable generation from multiple forecasting services and seeks a value-oriented combination of these forecasts to achieve lower cost in a two-stage unit commitment problem. We highlight two contributions. (a) We propose a value-oriented training of forecast combinations using PH alongside a faster PH modification that is scalable and allows high-fidelity training models. Relative to similar work in [3], [5] this enables the use of more historical data and avoids model approximations during training. As a result, and relative to similar work in [2], this allows solving the unit commitment problem in its standard form with binary variables in training. (b) Because our approach allows training with high-fidelity models we can analyze the impact of relaxing the decision-making problem in training.

II. PROBLEM DESCRIPTION

We consider a power system operator that manages a set of assets including wind turbines, large-scale generators, and flexible energy resources. To accommodate the dispatch lead time needed for large-scale generation units, the operator solves a two-stage problem. First, the operator solves a unit commitment (UC) problem on the day before the scheduled power delivery to accommodate planning lead times of some generators. Then, closer to actual power delivery, the operator solves a second “real-time” (RT) problem that uses the previously scheduled units and updated information on demand and renewable injection.

A. Unit commitment and real-time problem

The power system is modeled as a graph network with a set of nodes $i \in [N]$ (we write $[N] = \{1, \dots, N\}$) and lines (edges) $l \in [L]$. Every day d , the system operator first schedules production $p_{g,t,d}$ and commitment status $u_{g,t,d}$ for each timestep $t \in [T]$ and each generator $g \in [G]$. Schedules depend on uncertain net-load $L_{t,i,d}$ (i.e., load demand minus renewable injection) at time t on day d for node i . In the day-ahead UC the system operator uses a forecast $\hat{L}_{t,i,d}$ and the resulting problem is the mixed-integer linear program:

$$\text{UC}(\hat{L}_{t,i,d}) : \\ \min \sum_{g \in [G]} \sum_{t=2}^T (c_g^{SU} y_{g,t,d} + c_g^{SD} (u_{g,t-1,d} - u_{g,t,d} + y_{g,t,d})) +$$

The authors wish to thank the team of the Rutgers Center for Ocean Observation and Leadership (RUCOOL) for their help with data preparation.

$$\begin{aligned}
& \sum_{g \in [G]} \sum_{t=1}^T c_g p_{g,t,d} + \sum_{i \in [N]} \sum_{t=1}^T (c_i^{\text{shed}} \hat{l}_{i,t,d} + c_i^{\text{cur}} \hat{w}_{i,t,d}) \quad (1a) \\
\text{s.t. } & \sum_{g \in [G]} p_{g,t,d} + \sum_{l|r(l)=i} \hat{f}_{l,t,d} - \sum_{l|o(l)=i} \hat{f}_{l,t,d} = \hat{L}_{i,t,d} - \hat{l}_{i,t,d} \\
& \quad \forall t \in [T], \forall i \in [N] \quad (1b) \\
& \hat{f}_{l,t,d} = B_l (\hat{\theta}_{o(l),t,d} - \hat{\theta}_{r(l),t,d}) \quad \forall t \in [T], \forall l \in [L] \quad (1c) \\
& \hat{\theta}_{ref,t,d} = 0 \quad \forall t \in [T] \quad (1d) \\
& -\bar{F}_l \leq \hat{f}_{l,t,d} \leq \bar{F}_l \quad \forall t \in [T], \forall l \in [L] \quad (1e) \\
& \sum_{i=t-\bar{\ell}_g+1}^t y_{g,t,d} \leq u_{g,t,d} \quad \forall t \in [\bar{\ell}_g+1, T], \forall g \in [G] \quad (1f) \\
& \sum_{i=t-\underline{\ell}_g+1}^t y_{g,t,d} \leq 1 - u_{g,t-\underline{\ell}_g,d} \quad \forall t \in [\underline{\ell}_g+1, T], \forall g \in [G] \quad (1g) \\
& -u_{g,t-1,d} + u_{g,t,d} \leq y_{g,t,d} \quad \forall t \in [2, T], \forall g \in [G] \quad (1h) \\
& \underline{P}_g u_{g,t,d} \leq p_{g,t,d} \leq \bar{P}_g u_{g,t,d} \quad \forall t \in [1, T], \forall g \in [G] \quad (1i) \\
& p_{g,t,d} - p_{g,t-1,d} \leq R_g u_{g,t-1,d} + \bar{R}_g (1 - u_{g,t-1,d}) \\
& \quad \forall t \in [2, T], \forall g \in [G] \quad (1j) \\
& p_{g,t-1,d} - p_{g,t,d} \leq R_g u_{g,t,d} + \bar{R}_g (1 - u_{g,t,d}) \\
& \quad \forall t \in [2, T], \forall g \in [G] \quad (1k) \\
& 0 \leq \hat{l}_{i,t,d} \leq \max\{0, \hat{L}_{i,t,d} - \hat{W}_{i,t,d}\} \quad \forall i \in [N], \forall t \in [T] \quad (1l) \\
& 0 \leq \hat{w}_{i,t,d} \leq \hat{W}_{i,t,d} \quad \forall i \in [N], \forall t \in [T] \quad (1m) \\
& u_{g,t,d} \in \{0, 1\} \quad \forall g \in [G], \forall t \in [T] \quad (1n)
\end{aligned}$$

Objective (1a) minimizes the total generator production and start-up/shut-down cost (parametrized by c_g, c_g^{SU}, c_g^{SD}) and cost of load shedding $\hat{l}_{i,t,d}$ and curtailment $\hat{w}_{i,t,d}$ (parametrized by $c^{\text{shed}}, c^{\text{cur}}$). Eq. (1b) ensures that scheduled production meets the net demand forecast minus potential load shedding $\hat{l}_{i,t,d}$. Eq. (1c) models the power flow $\hat{f}_{l,t,d}$ over each line l as a function of line susceptance B_l and the difference between the voltage angle $\hat{\theta}_{i,t,d}$ at the node at the originating end of line l , i.e., $o(l)$, and the node at the receiving end of line l , i.e., $r(l)$. Constraint (1d) defines the voltage angle of the reference node and constraint (1e) transmission capacity limits \bar{F}_l . Constraints (1f), (1g) ensure generator minimum uptime $\bar{\ell}_g$ and downtime $\underline{\ell}_g$. In (1h), $y_{g,t,d}$ captures generator startup. Constraints (1i)–(1k) enforce lower and upper limits on power production ($\underline{P}_g, \bar{P}_g$) and ramping limits (R_g when online; \bar{R}_g when starting up) for each generator g depending on the binary unit commitment decision $u_{g,t,d} \in \{0, 1\}$. Lastly, constraints (1l) and (1m) establish the upper and lower limits on load shedding and renewable curtailment, respectively. For (1l) and (1m) we assume w.l.o.g. that the system operator can separate renewable forecasts $\hat{W}_{i,t,d}$ from the net-load forecasts.

1) Real-time problem

During real-time operations, the uncertain net-load materializes as $\bar{L}_{i,t,d}$ and the system operator manages energy imbalances that result from inaccurate forecasts by solving:

$$\text{RT}(p_{g,t,d}^*, u_{g,t,d}^*, \bar{L}_{i,t,d}) :$$

$$\begin{aligned}
\min & \sum_{g \in [G]} \sum_{t=1}^T (c_g^+ r_{g,t,d}^+ + c_g^- r_{g,t,d}^-) + \sum_{i \in [N]} \sum_{t=1}^T (c_i^{\text{shed}} l_{i,t,d} \\
& + c_i^{\text{cur}} w_{i,t,d}) \quad (2a) \\
\text{s.t. } & \sum_{g \in [G]} (p_{g,t,d}^* + r_{g,t,d}^+ - r_{g,t,d}^-) + \sum_{l|r(l)=i} f_{l,t,d} - \sum_{l|o(l)=i} f_{l,t,d} \\
& = \bar{L}_{i,t,d} - l_{i,t,d} \quad \forall t \in [T], \forall i \in [N] \quad (2b) \\
& f_{l,t,d} = B_l (\theta_{o(l)} - \theta_{r(l)}) \quad \forall t \in [T], \forall l \in [L] \quad (2c) \\
& \theta_{ref,t,d} = 0 \quad \forall t \in [T] \quad (2d) \\
& -\bar{F}_l \leq f_{l,t,d} \leq \bar{F}_l \quad \forall t \in [T], \forall l \in [L] \quad (2e) \\
& \underline{P}_g u_{g,t,d}^* \leq p_{g,t,d}^* + r_{g,t,d}^+ - r_{g,t,d}^- \leq \bar{P}_g u_{g,t,d}^* \quad \forall t \in [1, T], \\
& \quad \forall g \in [G] \quad (2f) \\
& (p_{g,t,d}^* + r_{g,t,d}^+ - r_{g,t,d}^-) - (p_{g,t-1,d}^* + r_{g,t-1,d}^+ - r_{g,t-1,d}^-) \\
& \leq R_g u_{g,t-1,d}^* + \bar{R}_g (1 - u_{g,t-1,d}^*) \quad \forall t \in [2, T], \forall g \in [G] \quad (2g) \\
& (p_{g,t-1,d}^* + r_{g,t-1,d}^+ - r_{g,t-1,d}^-) - (p_{g,t,d}^* + r_{g,t,d}^+ - r_{g,t,d}^-) \\
& \leq R_g u_{g,t,d}^* + \bar{R}_g (1 - u_{g,t,d}^*) \quad \forall t \in [2, T], \forall g \in [G] \quad (2h) \\
& 0 \leq r_{g,t,d}^-, r_{g,t,d}^+ \leq R_g \quad \forall g \in [G], \forall t \in [T] \quad (2i) \\
& 0 \leq \hat{l}_{i,t,d} \leq \max\{0, \bar{L}_{i,t,d} - \bar{W}_{i,t,d}\} \quad \forall i \in [N], \forall t \in [T] \quad (2j) \\
& 0 \leq w_{i,t,d} \leq \bar{W}_{i,t,d} \quad \forall i \in [N], \forall t \in [T] \quad (2k)
\end{aligned}$$

Values $p_{g,t,d}^*, u_{g,t,d}^*$ are the decisions obtained from UC. For given UC decisions $p_{g,t,d}^*, u_{g,t,d}^*$ and net-load realizations $\bar{L}_{i,t,d}$, the RT problem minimizes the cost of upward and downward redispatch ($r_{g,t,d}^+$ and $r_{g,t,d}^-$ with respective cost c_g^+ and c_g^-) such that the power balance in Eq. (2b) is ensured. Constraints (2f)–(2h) limit redispatch based on $p_{g,t,d}^*, u_{g,t,d}^*$ and the generation and ramping limits. The remaining constraints (2c)–(2k) are functionally equivalent to their analogous constraints in (1).

B. Optimal forecast combination

To solve UC, the system operator requires a single net-load forecast. We assume that the operator has access to net-load forecasts from multiple providers and must decide how to combine the information from these forecasts. We denote the combined net-load forecast as $\hat{L}_{i,t,d}^{\text{com}} = \sum_{k=1}^K \lambda_k \hat{L}_{i,t,d,k}$, where K is the number of forecast providers and λ_k is a provider-specific weight.

Typically, forecast quality is measured by how well it matches the observed value and numerous statistical methods exist to this end [8]. However, from the perspective of the two-stage UC and RT problem, a better metric for a good forecast combination, i.e., the choice of λ_k , is related to the cost of system operation resulting from the daily forecast-observation pair. Formally:

$$\lambda^* = \arg \min_{\lambda} \mathbb{E}_L \left[\text{UC} \left(\sum_{k=1}^K \lambda_k \hat{L}_k \right) + \text{RT}(\mathbf{p}^*, \mathbf{u}^*, \mathbf{L}) \right] \quad (3a)$$

$$\text{s.t. } \mathbf{p}^*, \mathbf{u}^* \in \arg \min UC \left(\sum_{k=1}^K \lambda_k \hat{L}_k \right). \quad (3b)$$

Bold variables indicate vectors, which we use to omit some indices for easier readability.

To determine a forecast combination that achieves the desired property in (3), we use historical forecasts and actual observations and formulate the bilevel training program:

$$\min_{\lambda_1, \dots, \lambda_K} \frac{1}{D} \left(\sum_{d=1}^D \{(1a) + (2a)\} \right) \quad (4a)$$

$$\text{s.t. } \hat{L}_d^{\text{comb}} = \sum_{k=1}^K \lambda_k \hat{L}_{k,d}, \quad \sum_{k=1}^K \lambda_k = 1 \quad (4b)$$

$$(2b) - (2k) \text{ [Real-time constraints]} \quad \forall d \in [D] \quad (4c)$$

$$\left. \begin{aligned} & p_d^*, u_d^* \in \left\{ \arg \min_{p_d, u_d} (1a) \right. \\ & \text{s.t. } \sum_{g \in [G]_i} p_{g,t,d} + \sum_{l|r(l)=i} \hat{f}_{l,t,d} - \sum_{l|o(l)=i} \hat{f}_{l,t,d} = \hat{L}_{i,t,d}^{\text{comb}} \\ & \quad - \hat{l}_{i,t,d} \quad \forall t \in [T], \forall i \in [N] \\ & (1c) - (1n) \text{ [Day-ahead UC constraints]} \end{aligned} \right\} \forall d \in [D]. \quad (4d)$$

Here, the upper-level problem finds a λ that minimizes the sample average two-stage operation cost over D days for which historical data is available. Constraint (4b) computes the combined forecast by assigning weight to each forecast vector and enforces a convex combination of forecasts [2]. The outer level problem also obtains the RT solution (4c) for a given realized net load \bar{L} and a given previous unit commitment decision p_d^*, u_d^* . The lower-level problem in (4d) solves the UC problem (1) and is parameterized by the combined forecast \hat{L}_d^{comb} .

III. SOLUTION METHODOLOGY

Problem (4) is hard to solve not only because it is a bilevel program but also because of the scale of practical power systems, binary variables in the lower-level UC problem, and the scaling with the number of historical training data. In the following, we first derive a single-level one-shot representation of (4) similar to [3], [5] as a benchmark. We then propose a more tractable solution alternative.

A. Single-level training problem

Typically, solving (4) involves replacing the lower-level (inner) problem with its Karush–Kuhn–Tucker (KKT) optimality conditions [3], [5]. However, the lower-level UC problem is non-convex due to its binary variables. To overcome this, we use a convex relaxation of UC that we denote UC-R.

1) Convex relaxation of binary variables

The relaxed UC-R is a primal formulation of the Lagrangian dual problem of UC [9] where the feasible set for each generator is replaced by its convex hull allowing the binary variable $u_{g,t,d}$ to be modeled continuous:

$$p_{g,t-1,d} \leq \bar{R}_g u_{g,t-1,d} + (\bar{P}_g - \bar{R}_g)(u_{g,t,d} - y_{g,t,d}) \quad \forall t \in [2, T], \forall g \in [G] \quad (5a)$$

$$p_{g,t,d} \leq \bar{P}_g u_{g,t,d} - (\bar{P}_g - \bar{R}_g) y_{g,t,d} \quad \forall t \in [2, T], \forall g \in [G] \quad (5b)$$

$$\begin{aligned} p_{g,t,d} - p_{g,t-1,d} &\leq (\underline{P}_g + R_g) u_{g,t,d} - \underline{P}_g u_{g,t-1,d} - \\ &(\underline{P}_g + R_g - \bar{R}_g) y_{t,d,g} \quad \forall t \in [2, T], \forall g \in [G] \end{aligned} \quad (5c)$$

$$\begin{aligned} p_{g,t-1,d} - p_{g,t,d} &\leq \bar{R}_g u_{g,t-1,d} - (\bar{R}_g - R_g) u_{g,t,d} - \\ &(\underline{P}_g + R_g - \bar{R}_g) y_{g,t,d} \quad \forall t \in [2, T], \forall g \in [G] \end{aligned} \quad (5d)$$

$$u_{g,t,d} \geq 0 \quad \forall t \in [T], \forall g \in [G] \quad (5e)$$

So, the resulting UC-R is:

$$\min (1a) \text{ s.t. } \{(1b) - (1m), (5a) - (5e)\} \quad (6)$$

2) KKT conditions

The KKT conditions of UC-R are:

$$\begin{aligned} & \nabla(1a) + \sum_{j \in [J]} \Psi_{g,t,d}^j \nabla f_j(p_{g,t,d}, u_{g,t,d}, y_{g,t,d}) \\ & + \sum_{b \in [B]} \Psi_{i,t,d}^b \nabla f_b(\hat{l}_{i,t,d}, \hat{w}_{i,t,d}) + \sum_{q \in [Q]} \Psi_{l,t,d}^q \nabla f_q(\hat{f}_{l,t,d}) \\ & + \nu_{i,t,d} \nabla h(\hat{f}_{l,t,d}, p_{g,t,d}) + \nu_{l,t,d} \nabla h(\hat{f}_{l,t,d}, \hat{\theta}_{i,t,d}) = 0 \end{aligned} \quad (7a)$$

$$(1b) - (1m), \quad (5a) - (5e) \quad \text{[Primal feasibility]} \quad (7b)$$

$$\Psi_{g,t,d}^j f_j(p_{g,t,d}, u_{g,t,d}, y_{g,t,d}) = 0 \quad \forall g \in [G], \forall j \in [J], \forall t \in [T] \quad (7c)$$

$$\Psi_{i,t,d}^b f_b(\hat{l}_{i,t,d}, \hat{w}_{i,t,d}) = 0 \quad \forall i \in [N], \forall b \in [B], \forall t \in [T] \quad (7d)$$

$$\Psi_{l,t,d}^q f_q(\hat{f}_{l,t,d}) = 0 \quad \forall l \in [L], \forall q \in [Q], \forall t \in [T] \quad (7e)$$

$$\Psi_{i,t,d}^b \geq 0 \quad \forall t \in [T], \forall i \in [N], \forall b \in [B] \quad (7f)$$

$$\Psi_{g,t,d}^j \geq 0 \quad \forall t \in [T], \forall g \in [G], \forall j \in [J] \quad (7g)$$

$$\Psi_{l,t,d}^q \geq 0 \quad \forall t \in [T], \forall l \in [L], \forall q \in [Q] \quad (7h)$$

where Ψ^b , Ψ^j , and Ψ^q are the Lagrange multipliers inequality constraints on each node i represented by $f_b(\cdot)$, each generator $g \in [G]$ represented by $f_j(\cdot)$, and each transmission line l represented by $f_q(\cdot)$. Values B , Q , and J denote the respective numbers of constraints/dual variables. Also, ν is the Lagrange multiplier related to equality constraints represented by $h(\cdot)$. The constraints (7a), (7b), (7c)–(7e), and (7f)–(7h) are, respectively, the stationarity, primal feasibility, complementary slackness, and dual feasibility conditions of the lower-level problem in (4).

We address the resulting non-linearity in the complementarity slackness conditions (7c)–(7e) using a regularization approach from [10]. This method replaces (7c)–(7e) with:

$$\forall d \in [D], \forall t \in [T] :$$

$$\sum_{j \in [J]} \Psi_{g,t,d}^j f_j(p_{g,t,d}, u_{g,t,d}, y_{g,t,d}) \leq \epsilon \quad \forall g \in [G] \quad (8a)$$

$$\sum_{b \in [B]} \Psi_{i,t,d}^b f_b(\hat{l}_{i,t,d}, \hat{w}_{i,t,d}) \leq \epsilon \quad \forall i \in [N] \quad (8b)$$

$$\sum_{q \in [Q]} \Psi_{l,t,d}^q f_q(\hat{f}_{l,t,d}) \leq \epsilon \quad \forall l \in [L]. \quad (8c)$$

Here, ϵ represents a small non-negative scalar that enables the reformulation of the KKT condition into a parametrized nonlinear problem that can be solved by modern off-the-shelf non-linear solvers. We denote this method as ST-N.

Alternatively, the complementarity slackness conditions can be linearized using Fortuny–Amat [11] (“Big-M”):

$$\forall t \in [T], \forall d \in [D] :$$

$$0 \leq \Psi_{g,t,d}^j \leq M z_{g,t,d}^j \quad \forall g \in [G], \forall j \in [J] \quad (9a)$$

$$0 \leq f_j(\hat{f}_{g,t,d}) \leq M(1 - z_{g,t,d}^j) \quad \forall g \in [G], \forall j \in [J] \quad (9b)$$

$$0 \leq \Psi_{i,t,d}^b \leq M z_{i,t,d}^b \quad \forall i \in [N], \forall b \in [B] \quad (9c)$$

$$0 \leq f_b(\hat{f}_{i,t,d}) \leq M(1 - z_{i,t,d}^b) \quad \forall i \in [N], \forall b \in [B] \quad (9d)$$

$$0 \leq \Psi_{l,t,d}^q \leq M z_{l,t,d}^q \quad \forall l \in [L], \forall q \in [Q] \quad (9e)$$

$$0 \leq f_q(\hat{f}_{l,t,d}) \leq M(1 - z_{l,t,d}^q) \quad \forall l \in [L], \forall q \in [Q] \quad (9f)$$

where z are binary variables, and $M \in \mathbb{R}^+$ is a large enough constant. We denote this method as ST-M.

3) Single-level equivalent

The resulting single-level equivalent of (4) is:

$$\begin{aligned} \min_{\lambda_1, \dots, \lambda_K} \quad & (4a) \\ \text{s.t.} \quad & (4b) - (4c), \quad (7a) - (7b), \quad (7f) - (7h) \quad (10) \\ & (8a) - (8c) \text{ for ST-N or } (9a) - (9f) \text{ for ST-M.} \end{aligned}$$

The training problem in (10) solves a two-level network-constrained problem for each time t over all days d and includes binary or non-linear structures. Therefore, this problem cannot be expected to be computationally tractable for practical application. To resolve this issue, we propose a PH algorithm, in which we decompose (10) into D sub-problems and solve each of them independently.

B. Progressive Hedging Algorithm

Progressive hedging (PH), introduced in [12], decomposes the original problem such that each scenario (day of training data in our case) can be solved independently and then uses an augmented Lagrangian approach to achieve consensus between shared variables. This structure makes the algorithm particularly suited for parallelization and drastically reduces the size of each individual problem, allowing for efficient simultaneous computations. Moreover, because the PH problem solves the two-stage UC and RT problem individually for each day, we do not require the KKT conditions of the UC problem and can instead formulate a combined UC and RT problem using their primal formulations (1) and (2):

$\text{PH}(\hat{\mathbf{L}}_d, \boldsymbol{\mu}, \rho, \bar{\boldsymbol{\lambda}})$:

$$\min_{\boldsymbol{\lambda}_d} (1a) + (2a) + (\boldsymbol{\mu}_d^{\tau-1})^T \boldsymbol{\lambda}_d + \frac{\rho}{2} \|\boldsymbol{\lambda}_d - \bar{\boldsymbol{\lambda}}^{\tau-1}\|^2 \quad (11a)$$

$$\text{s.t.} \quad \hat{\mathbf{L}}_d^{\text{comb}} = \sum_{k=1}^K \lambda_{d,k} \hat{\mathbf{L}}_{d,k}, \quad \sum_{k=1}^K \lambda_{d,k} = 1 \quad (11b)$$

$$\begin{aligned} \sum_{g \in [G]_i} p_{g,t,d} + \sum_{l|r(l)=i} \hat{f}_{l,t,d} - \sum_{l|o(l)=i} \hat{f}_{l,t,d} \\ = \hat{\mathbf{L}}_{i,t,d}^{\text{comb}} - \hat{l}_{i,t,d} \quad \forall t \in [T], \forall i \in [N] \end{aligned} \quad (11c)$$

$$(1c) - (1n) \quad [\text{Day-ahead UC constraints}] \quad (11d)$$

$$(2b) - (2k) \quad [\text{Real-time constraints}] \quad (11e)$$

In this formulation, we again use bold symbols to denote vectors. Problem (11) is solved for each day and in each iteration of the PH algorithm. In essence, each day computes its individual optimal forecast combination $\boldsymbol{\lambda}_d$ based on the data for that day. The PH algorithm then computes the

average forecast combination $\bar{\boldsymbol{\lambda}}$ and each day recomputes its optimal forecast combination with additional PH penalty factors $\boldsymbol{\mu}_d$ and ρ that are added to the objective (11a). We can solve (11) using both UC and UC-R models. To solve (11) with UC-R, we replace equations (1c)–(1n) with (1c)–(1m), (5a)–(5e) in (11d).

Alg. 1 shows the PH method in detail. After initialization, a so-called PH multiplier $\boldsymbol{\mu}_d$ is calculated for each training day d based on the difference between the individual $\boldsymbol{\lambda}_d$ and the average $\bar{\boldsymbol{\lambda}}$ computed across all days (Line 5 in Alg. 1). Each day then re-solves (11) parametrized by the current PH multiplier $\boldsymbol{\mu}_d$ and the average $\bar{\boldsymbol{\lambda}}$ from the previous solution. (Line 8 in Alg. 1). These steps are repeated until the total consensus gap g (Line 11 in Alg. 1) is smaller than a predefined threshold ϵ .

Algorithm 1 PH Algorithm

```

1: Input:  $\{\rho > 0, \epsilon > 0, \hat{\mathbf{L}}, \bar{\mathbf{L}}\}$ 
2: Initialization:
3:    $\boldsymbol{\lambda}_d^0 \leftarrow \text{PH}(\hat{\mathbf{L}}_d, 0, 0, 0), \forall d \in [D]$   $\triangleright$  Solves (11)
4:    $\bar{\boldsymbol{\lambda}}^0 \leftarrow \frac{1}{D} \sum_{d \in [D]} \boldsymbol{\lambda}_d^0$   $\triangleright$  Average weights
5:    $\boldsymbol{\mu}_d^0 \leftarrow \rho(\boldsymbol{\lambda}_d^0 - \bar{\boldsymbol{\lambda}}^0), \forall d \in [D]$   $\triangleright$  Initial PH multipliers
6:    $\tau = 1$   $\triangleright$  Set iteration counter
7:   repeat
8:      $\boldsymbol{\lambda}_d^\tau \leftarrow \text{PH}(\hat{\mathbf{L}}_d, \boldsymbol{\mu}_d^{\tau-1}, \rho, \bar{\boldsymbol{\lambda}}^{\tau-1}), \forall d \in [D]$   $\triangleright$  Solves (11)
9:      $\bar{\boldsymbol{\lambda}}^\tau \leftarrow \frac{1}{D} \sum_{d \in [D]} \boldsymbol{\lambda}_d^\tau$   $\triangleright$  Average weights
10:     $\boldsymbol{\mu}_d^\tau \leftarrow \boldsymbol{\mu}_d^{\tau-1} + \rho(\boldsymbol{\lambda}_d^\tau - \bar{\boldsymbol{\lambda}}^\tau), \forall d \in [D]$   $\triangleright$  Current PH multipliers
11:     $g^\tau \leftarrow \sum_{d \in [D]} \|\boldsymbol{\lambda}_d^\tau - \bar{\boldsymbol{\lambda}}^\tau\|$   $\triangleright$  Current convergence
12:     $\tau \leftarrow \tau + 1$   $\triangleright$  Step iteration counter
13:  until  $g^\tau < \epsilon$ 

```

Algorithm 2 Selective PH Algorithm (SPH)

```

1: Input:  $\{\rho > 0, \epsilon > 0, \hat{\mathbf{L}}, \bar{\mathbf{L}}, D'\}$ 
2: [Lines 2–6 of Alg. 1]
3: repeat
4:    $ds_d \leftarrow \|\boldsymbol{\lambda}_d^{\tau-1} - \bar{\boldsymbol{\lambda}}^{\tau-1}\|, \forall d \in [D]$   $\triangleright$  Deviation score
5:   Find  $\mathcal{S}', \bar{\mathcal{S}}'$  such that  $\mathcal{S}' \subseteq [D], |\mathcal{S}'| = D', \bar{\mathcal{S}}' = [D] \setminus \mathcal{S}'$ 
   where  $\forall i \in \mathcal{S}', \forall j \in \bar{\mathcal{S}}' : ds_i \geq ds_j$ 
6:    $\boldsymbol{\lambda}_d^\tau \leftarrow \text{PH}(\hat{\mathbf{L}}_d, \boldsymbol{\mu}_d^{\tau-1}, \rho, \bar{\boldsymbol{\lambda}}^{\tau-1}), \forall d \in \mathcal{S}'$   $\triangleright$  Solves (11)
7:    $\boldsymbol{\lambda}_d^\tau \leftarrow \boldsymbol{\lambda}_d^{\tau-1}, \forall d \in \bar{\mathcal{S}}'$ 
8:   [Lines 9–12 of Alg. 1]
9: until  $g^\tau < \epsilon$ 

```

C. Selective Progressive Hedging

In each iteration, the PH algorithm re-solves all training days. (See Line 8 in Alg. 1.) We can speed up the PH approach through a variant of Alg. 1, where we select a smaller subset $\mathcal{S}' \subseteq [D]$ of the days to be re-evaluated at each iteration (Line 6 in Alg. 2). To this end, we compute a deviation score $ds_d = \|\boldsymbol{\lambda}_d^{\tau-1} - \bar{\boldsymbol{\lambda}}^{\tau-1}\|$ at each iteration and select the indices of the D' largest deviation scores to create \mathcal{S}' . We also define $\bar{\mathcal{S}}' := [D] \setminus \mathcal{S}'$. (See line 5 in Alg. 2.) At each iteration, only the $\boldsymbol{\lambda}_d$ for $d \in \mathcal{S}'$ are re-computed. This allows to control of the per-iteration computational cost to achieve fast iterations at a potential longer convergence time.

IV. NUMERICAL EXPERIMENTS

We first test our method in detail on the IEEE 24-bus test system [13] using real-world offshore wind data from two

different forecasting sources. We then apply the method to the 2736-bus Polish system [14] to highlight scalability.

A. Description of experiments and data

We first focus on the IEEE 24-bus test system. We use real-world demand profiles from ENTSO-E [15] and two data sources for uncertain wind power injections from the Rutgers University Center for Ocean Observing Leadership (RUCOOL) [16], [17] and the NREL NOW23 data set [18]. Each dataset contains hourly day-ahead forecasts and actuals for wind speed, which we translated to wind power using the NREL 15-Megawatt Reference Wind Turbine [19]. We note that here we model demand as deterministic and only wind as uncertain. This, however, is no advantage for the performed computations. We locate wind farms at nodes 3, 5, 9, 16, 19, 20 and the capacity of each wind farm is 400 MW. We set $c_i^{\text{cur}} = \$50/MWh$, $\forall i$ and $c_i^{\text{shed}} = \$25,000/MWh$, $\forall i$. The time horizon is 24 hours and $K = 2$, i.e., $k = 1$ for RUCOOL and $k = 2$ for NOW23. We set $D' = \lceil 1/3D \rceil$. We choose ρ by solving Alg. 1 with various ρ and used reference results from solving (4) (see discussion below) to select $\rho = 25,000$. We set $\epsilon = 10^{-5}$ for PH and SPH.

All computations have been implemented in Julia using JuMP [20] and solved using the Gurobi solver [21] on the Rutgers Amarel cluster on nodes with 128 GB of memory and 16 cores (Dual Intel Xeon Gold 6448Y processors).

B. Small-scale reference cases

We first solve (10) in the ST-M and ST-N variants to obtain reference solutions and gauge the scalability of this direct approach. The largest instance that could be solved without running out of memory or hitting a limit of three computation days used 30 days of historical data. We therefore used an instance of the problem with one month worth of training days to compare ST-M and ST-N with the PH methods. Table I summarizes the results. Values for PH and SPH have been obtained by solving Alg. 1 and Alg. 2, respectively, with the UC-R variant of (11). We do this for better comparability because ST-M and ST-N inherently require UC-R.

We observe that the resulting forecast combinations λ_1 and λ_2 are similar across the methods and confirm the correct convergence of PH and SPH. See also the top plot in Fig. 1. Table I also shows the required training time. Clearly, the PH and SPH approaches outperform the ST-M and ST-N methods in terms of computational speed. ST-N and PH are similar, but ST-M failed to scale to larger problem instances.

We test the performance of the obtained forecast combination by running the two-stage UC+RT problem (UC in its standard form with binary variables) for one year with different forecast combinations: (a) $\lambda_1 = 1$, $\lambda_2 = 0$ (using only forecasts from forecast provider 1), (b) $\lambda_1 = 0$, $\lambda_2 = 1$ (using only forecasts from forecast provider 2), and (c) $\lambda_1 = 0.5$, $\lambda_2 = 0.5$ (using the naive average). We define the resulting average two-stage cost as $\text{TST}(\lambda_1, \lambda_2)$. We denote the average testing results using the value-oriented forecast as TST^* . In Table I, columns Δ_a , Δ_b , Δ_c then show the average daily improvement the value-oriented forecast

TABLE I
RESULTS OF 4 DIFFERENT SOLUTION METHODS FOR ONE MONTH.

Method	λ_1^*	λ_2^*	Time (s)	TST* [\$]	Δ_a	Δ_b	Δ_c
ST-M	0.464	0.535	64800	3645874	-66625	-58291	-3171
ST-N	0.462	0.537	2368	3644656	-67843	-59508	-4388
PH (CR)	0.471	0.528	2149	3640312	-72187	-63853	-8733
SPH (CR)	0.466	0.533	1943	3643742	-68757	-60422	-5302

Δ_a : $\text{TST}^* - \text{TST}(1,0)$, Δ_b : $\text{TST}^* - \text{TST}(0,1)$, Δ_c : $\text{TST}^* - \text{TST}(0.5,0.5)$

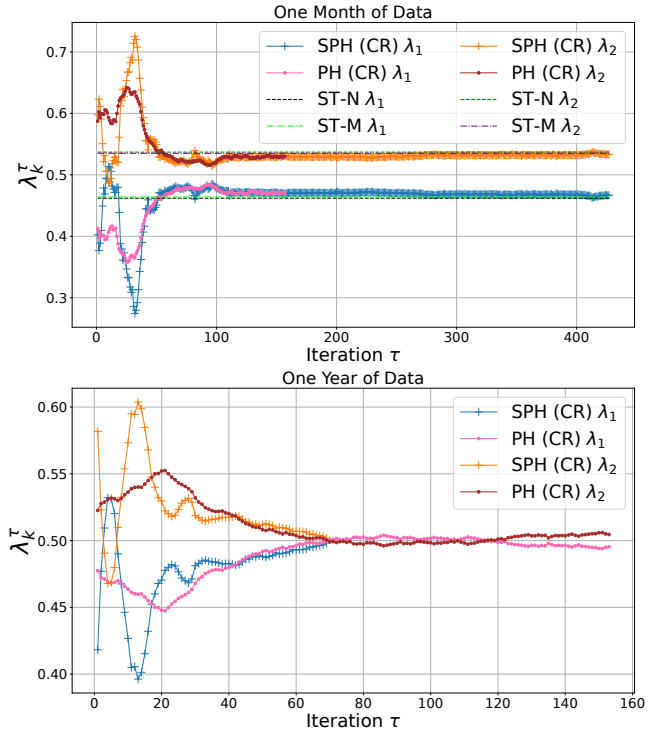


Fig. 1. Convergence of λ_k^τ for PH (CR) and SPH (CR) using one month (top) and one year (bottom) of training data. Top plot shows comparison with λ_{k-s} obtained from ST-M and ST-N.

achieves over the reference methods (a), (b), (c). In all cases, TST^* improves the solution, indicating systematic benefits of using the value-oriented forecast from any method.

C. PH algorithm with full training dataset

We now investigate modifications of the PH approach using all the available training data (one year). For this dataset, the direct training approaches ST-M and ST-N solving (10) were intractable and are no longer considered. We study the following modifications: As above, (S)PH (CR) solves Algs. 1, 2 using the UC-R version of (11). (S)PH (B) uses the standard formulation of UC with binary variables as written in (11) for Algs. 1, 2. For comparison with [3], we also solve a training version without network constraints in the UC stage. This is denoted N (with network) and NN (no network) in Table II, which summarizes the results.

SPH reduces the solution time of PH without much compromise in the solution, making large-scale problems tractable. Additionally, Fig. 1 shows the convergence speed of PH and SPH in different time periods. While SPH is slightly less stable in earlier iterations, it shows similar

TABLE II
RESULTS FOR ONE YEAR OF DATA

Method	λ_1^*	λ_2^*	Time (s)	TST* [\$]	Δ_a	Δ_b	Δ_c
PH (B)	0.502	0.497	26357	1806985	-40048	-45146	-7671
SPH (B)	0.501	0.498	3967	1805905	-41128	-46226	-8751
N PH (CR)	0.495	0.504	11301	1805192	-41841	-46939	-9464
SPH (CR)	0.498	0.501	4225	1805590	-41443	-46541	-9066
NN PH (B)	0.453	0.547	10956	1816795	-30238	-35336	2139
NN SPH (B)	0.488	0.512	4954	1820322	-26711	-31809	5666
RMSE	0.483	0.517	0	1840149	-6884	-11982	25493

TABLE III
RESULTS OF SPH FOR 2736 BUS SYSTEM

Time Period	λ_1^*	λ_2^*	Time (s)	TST* [\$]	Δ_c
one month	0.002	0.998	17640	117440	-1167
one year	0.643	0.356	73740	113965	-606

convergence behavior as PH. In fact, it meets the convergence criterion faster than PH. Fewer iterations also explain the faster training of SPH (B) over SPH (CR).

We observe that forecast combinations strictly improve the decision value. Interestingly, using the convex hull version of the UC problem in training leads to the best improvements in (S)PH (CR). We suspect that the PH algorithm benefits from the convexity of the underlying problem. Training the forecast combination network-ignorant (rows NN in Table II) improves upon using a single forecast, but performs worse in testing than just averaging the forecasts. Here, ignoring network congestion in training creates an advantage for the forecasts from forecast provider 2, which tends to underestimate hourly wind power fluctuations.

D. Comparison to statistical method

We compare our value-oriented forecast combination with an established statistics-based combination method based on the root mean square errors (RMSE) of the forecasts [22]. For each $k \in [K]$ we compute the RMSE as

$$\text{RMSE}_k = \left(\frac{1}{D} \sum_{d=1}^D \left(\frac{1}{N \times T} \sum_{i=1}^N \sum_{t=1}^T (\hat{L}_{i,t,d,k} - \bar{L}_{i,t,d})^2 \right) \right)^{\frac{1}{2}} \quad (12)$$

and then calculate λ_k inversely proportional to the RMSE as $\lambda_k = \frac{\text{RMSE}_k}{\sum_{k=1}^K \text{RMSE}_k}$ [22]. The resulting RMSE of the combined forecast using this method is 0.379. Notably, the RMSE of the value-oriented forecast obtained with PH (B) is higher with 0.382. Yet, as we observe in row RMSE in Table II, the value-oriented forecasts systematically improve upon the RMSE method. PH (B) achieves a cost saving of \$33164.

E. Scalability

We test the scalability of the proposed method, by running SPH (CR) for the 2736-bus Summer Peak Polish system from [14] to which we added 21 wind farms with 400MW capacity each. We used the same data for load and wind forecasts as described in Section IV-A above. Table III summarizes the results. The training time remains manageable. Even for one full year of historical data, the algorithm converges after about 20h and improves the outcome in testing.

V. CONCLUSION

We presented a method for value-oriented forecast combinations using progressive hedging (PH), unlocking high-fidelity, at-scale models and large-scale datasets in training. We derived a one-shot reference model and discussed its scaling issues and presented the proposed PH approach alongside a modification that further reduces computation time. Our case study demonstrated the usefulness of value-oriented forecast combinations and showed the scalability of the the proposed method. Unit commitment and real-time dispatch cost were reduced by 1.8% on average and we were able to obtain forecast combinations for the 2736 Polish system using a full year of historical data within 20 hours. The method presented in this paper unlocks follow-up research on more context-aware forecast combination models as well as options to train models that provide advanced insights, such as forecast purchasing decisions.

REFERENCES

- [1] T. Carriere *et al.*, "An integrated approach for value-oriented energy forecasting and data-driven decision-making application to renewable energy trading," *IEEE Trans. Smart Grid*, vol. 10, no. 6, 2019.
- [2] A. Stratigakos *et al.*, "Decision-focused linear pooling for probabilistic forecast combination," *International Journal of Forecasting*, 2024.
- [3] J. M. Morales *et al.*, "Prescribing net demand for two-stage electricity generation scheduling," *Oper. Res. Perspect.*, vol. 10, 2023.
- [4] P. Donti *et al.*, "Task-based end-to-end model learning in stochastic optimization," *Adv. Neural Inf. Process. Syst.*, vol. 30, 2017.
- [5] Y. Zhang *et al.*, "Toward value-oriented renewable energy forecasting: An iterative learning approach," *IEEE Trans. Smart Grid*, 2024.
- [6] J. Dias Garcia *et al.*, "Application-driven learning: A closed-loop prediction and optimization approach applied to dynamic reserves and demand forecasting," *Oper. Res.*, vol. 73, no. 1, 2025.
- [7] R. Mieth *et al.*, "Prescribed robustness in optimal power flow," *Electric Power Systems Research*, vol. 235, 2024.
- [8] X. Wang *et al.*, "Forecast combinations: An over 50-year review," *International Journal of Forecasting*, vol. 39, no. 4, 2023.
- [9] B. Hua *et al.*, "A convex primal formulation for convex hull pricing," *IEEE Trans. Power Syst.*, vol. 32, no. 5, 2016.
- [10] S. Scholtes, "Convergence properties of a regularization scheme for mathematical programs with complementarity constraints," *SIAM J. Optim.*, vol. 11, no. 4, 2001.
- [11] J. Fortuny-Amat *et al.*, "A representation and economic interpretation of a two-level programming problem," *Journal of the operational Research Society*, vol. 32, no. 9, 1981.
- [12] R. T. Rockafellar *et al.*, "Scenarios and policy aggregation in optimization under uncertainty," *Math. Oper. Res.*, vol. 16, no. 1, 1991.
- [13] MATPOWER. (2016) Case24 IEEE RTS. [Online]. Available: https://matpower.org/docs/ref/matpower6.0/case24_ieee_rts.html
- [14] R. D. Zimmerman *et al.*, "Matpower: Steady-state operations, planning, and analysis tools for power systems research and education," *IEEE Trans. Power Syst.*, vol. 26, no. 1, 2010.
- [15] Open Power System Data Platform. [Online]. Available: <https://data.open-power-system-data.org/>
- [16] J. Dicapoulos *et al.*, "Weather research and forecasting model validation with nrel specifications over the new york/new jersey bight for offshore wind development," in *OCEANS 2021*. IEEE, 2021.
- [17] RUCOOL. (2019) Rutgers weather research and forecasting model. Accessed: 2025-03-10. [Online]. Available: https://tds.marine.rutgers.edu/thredds/dodsC/cool/rurwrf/wrf_4.1_3km_processed/WRF_4.1_3km_Processed_Dataset_Best.html
- [18] N. Bodini *et al.* (2020) 2023 national offshore wind data set (now-23). [Online]. Available: <https://data.openei.org/submissions/4500>
- [19] E. Gaertner *et al.*, "Iea wind tep task 37: definition of the ie15-megawatt offshore reference wind turbine," National Renewable Energy Lab.(NREL), Golden, CO (United States), Tech. Rep., 2020.
- [20] M. Lubin *et al.*, "Jump 1.0: Recent improvements to a modeling language for mathematical optimization," *Math. Program. Comput.*, vol. 15, no. 3, 2023.

- [21] Gurobi Optimization, LLC, "Gurobi Optimizer Reference Manual," 2024. [Online]. Available: <https://www.gurobi.com>
- [22] J. Nowotarski *et al.*, "An empirical comparison of alternative schemes for combining electricity spot price forecasts," *Energy Economics*, vol. 46, 2014.